

Enhanced Tumor Accumulation of Sub-2 nm Gold Nanoclusters for Cancer Radiation Therapy

Xiao-Dong Zhang¹, Jie Chen¹, Zhentao Luo², Di Wu¹, Xiu Shen¹, Sha-Sha Song¹, Yuan-Ming Sun¹, Pei-Xun Liu¹, Jing Zhao³, Shuaidong Huo³, Saijun Fan¹, Feiyue Fan¹, Xing-Jie Liang^{3*}, and Jianping Xie^{3*}

¹Tianjin Key Laboratory of Molecular Nuclear Medicine, Institute of Radiation Medicine, Chinese Academy of Medical Sciences and Peking Union Medical College, Tianjin, 300192, China

²Department of Chemical and Biomolecular Engineering, National University of Singapore, 10 Kent Ridge Crescent, 119260, Singapore

³CAS Key Laboratory for Biological Effects of Nanomaterials and Nanosafety, National Center for Nanoscience and Technology, Beijing, 100190, China

Email: chexiej@nus.edu.sg

Email: liangxj@nanoctr.cn

Keywords: gold nanoclusters, radiation therapy, radiosensitizers, renal clearance, *in vivo* treatment

Abstract: A new type of *metabolizable* and *efficient* radiosensitizer for cancer radiotherapy is presented in this study by combining ultrasmall Au nanoclusters (NCs, <2 nm) with biocompatible coating ligands (glutathione, GSH). The new nano-construct (GSH-coated Au₂₅ NCs) inherits attractive features of both the Au core (strong radiosensitizing effect) and GSH shell (good biocompatibility). It can preferentially accumulate in tumor *via* the improved EPR effect, which leads to strong enhancement for cancer radiotherapy. After the treatment, the small-sized GSH-Au₂₅ NCs can be efficiently cleared by the kidney, minimizing any potential side effects due to the accumulation of Au₂₅ NCs in the body.

1. Introduction

Gold nanoparticles (Au NPs) possess distinct physical and chemical properties that make them ideal platforms for a variety of biomedical applications, including imaging, biosensing, drug delivery, and therapy.^[1] Recently, Au NPs have been applied as a promising new type of radiotherapy sensitizing agents (or radiosensitizers) for cancer treatment because of their strong absorption and high efficiency in generating secondary electrons under gamma ray or X-ray irradiation, enhancing the DNA and protein damages in tumors.^[2] A good radiosensitizer must feature two properties: (1) efficient accumulation in tumors during the radiation treatment to achieve sufficient enhancement for the radiotherapy, and (2) effective renal clearance after the treatment to minimize toxic side effects. Here we report a novel type of Au NP-based radiosensitizers: ultrasmall Au NPs (<2 nm) protected by naturally occurring biomolecules (e.g., peptides and proteins). The complementary features of the two key components, the sub-2 nm Au core and the biomolecule coating, are integrated into a single entity, that is, biomolecule-coated ultrasmall Au NPs, to achieve targeted properties of a good radiosensitizer.

Ultrasmall Au NPs were chosen in this study as the radiosensitizer. Sub-2 nm Au NPs, or termed Au nanoclusters (NCs), are a subgenre of NPs with a core size below 2 nm typically containing less than 150 Au atoms.^[3] Recent studies have shown that the accumulation efficiency of Au NPs in tumors was largely determined by the particle size, and smaller Au NPs have higher efficient tumor deposition. For example, it is well-documented that Au NPs with sizes >50 nm cannot pass through the outside barrier of the reticuloendothelial system (RES) but to form large aggregates (>100 nm) during the blood circulation, which led to a poor deposition of NPs in tumors.^[4] In contrast, Au NPs with sizes <50 nm showed radiation enhancement effects to a certain extent, suggesting the accumulation of the NPs in tumors.^{[2a,}

^{5]} In addition, 12 nm Au NPs coated with polyethylene glycol (PEG) showed obviously higher accumulation in tumors than those of 27.6 and 46.6 nm PEG-coated Au NPs.^[2b, 6] It is therefore expected that the ultrasmall Au NCs (< 2 nm) may have improved accumulation in tumors because of their enhanced permeability and retention (EPR) effect relative to that of large NPs (>2 nm),^[7] leading to an improved enhancement for cancer radiotherapy.

Coating ligands on the NP surface can also affect the pharmacokinetics of Au NPs in the body by controlling the surface chemistry and hydrodynamic diameter (HD) of the Au NPs, which are two primary factors that can affect the properties and behavior of Au NPs under physiological conditions.^[8] For example, 3 nm Au NPs coated with different ligands showed different colloidal stability in the body: the PEG-coated Au NPs were not stable and formed aggregates in blood, whereas the glutathione (GSH)-coated Au NPs were highly stable under the same conditions.^[9] The different behaviors of Au NPs in blood may lead to different deposition efficiencies in tumors. Due to the ultrasmall size of Au NCs, the effect of coating ligands on their pharmacokinetics in the body could be more pronounced than that of larger NPs.^[10] In addition, the biocompatibility of the coating ligands on the NP surface is a key consideration for all biomedical applications, and a good compliance strategy is to select a naturally occurring biomolecule as the coating ligand.^[11] The natural peptide – GSH and the bovine serum albumin (BSA) are widely used as biocompatible coating ligands for Au NPs in various biomedical settings. Therefore, we hypothesized that an efficient and safe radiosensitizer could be constructed by incorporating biocompatible ligands (GSH or BSA) into the ultrasmall Au NCs, forming GSH- or BSA-coated Au NCs, which may have improved passive tumor targeting performance *via* the EPR effect.

One concern related to the therapeutic Au NPs is biosafety. Au NPs are generally considered as safe materials in view of their good biocompatibility and low *in vitro* cytotoxicity.

However, Au NPs with a relatively large size (>10 nm) cannot be metabolized and tend to be absorbed by RES and accumulate in liver and spleen, which leads to potential damages to the liver and immune system.^[12] Recent studies suggested that the HD of the NPs could determine the renal clearance efficiency.^[9a] For example, semiconductor quantum dots (QDs) with a HD <5.5 nm was rapidly and efficiently removed by the kidney, whereas QDs with a HD >15 nm did not show efficient renal excretion and were accumulated in the liver and spleen.^[13] Similarly, the GSH-coated Au NPs with particle size in the range of 1.5–3 nm showed high efficiency in the renal clearance.^[9-10]

This article is an account of our investigation of the GSH- and BSA-coated Au NCs for cancer radiotherapy. The well-studied Au₂₅ NCs species was chosen as the model of the new NC-based radiosensitizers because of their ultrasmall size (<2 nm) and excellent chemical stability. *In vitro* and *in vivo* studies of the GSH- and BSA-coated Au₂₅ NCs (or GSH- and BSA-Au₂₅ NCs for short) for cancer radiotherapy are presented here with detailed analyses of the cell response, DNA damage, and changes in tumor volume and weight after the treatment. *In vivo* cytotoxicity of GSH-Au₂₅ NCs was investigated with experimental evidences from the pathology, biochemistry, organ index, and biodistribution studies. Our findings suggest that GSH-Au₂₅ NCs are promising radiosensitizers for cancer radiotherapy with attractive features including excellent tumor accumulation, strong radiation enhancement, and low toxicity (efficient renal clearance).

2. Results and Discussion

GSH- and BSA-Au₂₅ NCs were synthesized and purified according to published procedures.^[14] Both types of the NCs have a core-shell structure, as illustrated in **Figure 1a** and **1b**. GSH-Au₂₅ NCs, which can be denoted as Au₂₅(SG)₁₈, have molecular-like absorptions due to the strong quantum confinement of free electrons in the ultrasmall particles.^[15] As shown in **Figure 1c** (black line), the GSH-Au₂₅ NCs showed the UV-vis absorption spectrum with a maximum at 670 nm and a few shoulder peaks that matched well with earlier studies.^[3d, 16] The well-defined absorption spectrum suggested the high purity of our sample. The ultrasmall size of GSH-Au₂₅ NCs was demonstrated by the transmission electron microscopy (TEM) image (**Figure 1e**), in which only particles smaller than 1.5 nm were observed. BSA-Au₂₅ NC consists of 25 Au atoms encapsulated by a BSA molecule (**Figure 1b**). Unlike GSH-Au₂₅ NCs, BSA-Au₂₅ NCs showed no obvious peaks in its UV-vis absorption spectrum (**Figure 1c**, red line). The distinctive difference in the absorptions of GSH- and BSA-Au₂₅ NCs is a result of the strong effects from the different coating ligands and protection chemistries, which are more pronounced in the ultrasmall NCs than in large NPs.^[14a, 17] As suggested by the TEM image (**Figure 1f**), the core size of BSA-Au₂₅ NCs was also below 1.5 nm, similar to that of GSH-Au₂₅ NCs. However, GSH- and BSA-Au₂₅ NCs showed very different HDs in dynamic light scattering (DLS) measurements. The HD of GSH-Au₂₅ NCs was ~2.4 nm (**Figure 1d**, black line), which was determined by the small size of the GSH ligand [molecular weight (MW) = 307]. In contrast, the BSA-Au₂₅ NCs had a HD of ~6 nm, which matched nicely with the size of BSA (MW ~66 kDa and HD ~6 nm) because the Au atoms were encapsulated by a single BSA molecule for each BSA-Au₂₅ NC.

The cell responses (or biocompatibility) of GSH- and BSA-Au₂₅ NCs were evaluated using the HeLa cells. The HeLa cell culture was first treated with GSH- or BSA-Au₂₅ NCs at different concentrations of 0.00625–0.2 mg-Au/mL. As shown in **Figure 2a**, after 24 and 48 h,

the viability of the cells changed very little with increasing NC concentration. The results showed that both GSH- and BSA-Au₂₅ NCs had low cytotoxicity even at a high dosage of 0.2 mg-Au/mL (after 48 h, the cell viability was ~85% and ~70% for GSH- and BSA-Au₂₅ NCs, respectively). The data also suggested that GSH-Au₂₅ NCs had better biocompatibility than that of BSA-Au₂₅ NCs. The good biocompatibility of GSH- and BSA-Au₂₅ NCs is expected because both GSH and BSA are naturally occurring benign biomolecules.

The radiation enhancements of GSH- and BSA-Au₂₅ NCs were measured by the colony formation assay using the Hela cells. As shown in Figure 2b, an obvious enhancement in radiation was observed for cell cultures treated with the GSH- or BSA-Au₂₅ NCs. In particular, the sensitization enhancement ratio (SER) of GSH-Au₂₅ NCs was ~1.30, which was higher than that of BSA-Au₂₅ NCs (~1.21) for all the radiation doses. The radiation enhancement effects of GSH- and BSA-Au₂₅ NCs may be due to the enhanced DNA damage induced by the photoelectric effect and Compton scattering of the heavy metal, that is, Au. This hypothesis was supported by the single-cell gel electrophoresis study. As shown in Figure 2c, without radiation, negligible DNA damage was observed for the cell cultures treated with GSH- and BSA-Au₂₅ NCs. This data provided yet another line of evidence for low cytotoxicity of both GSH- and BSA-Au₂₅ NCs. In contrast, after receiving a 3 Gy radiation dose, a significant DNA damage was observed for cell cultures treated with GSH- and BSA-Au₂₅ NCs (Figure 2c). The remarkable DNA damage was also suggested by the *in vitro* imaging with fluorescent DNA stain, in which a long tail indicated significant DNA damage. There was no obvious DNA damage observed in the control and NCs without radiation groups (Figure S1). As compared with the cell culture treated by radiation only (Figure 2d), cell cultures treated with GSH- or BSA-Au₂₅ NCs *plus* radiation (3 Gy) showed more significant DNA damages (Figure 2e and 2f). In addition, GSH-Au₂₅ NCs showed stronger radiation enhancement than BSA-Au₂₅ NCs, which could be attributed to the

improved cell uptake of the hydrodynamically smaller GSH-Au₂₅ NCs (HD ~2.4 nm) relative to that of the BSA-Au₂₅ NCs (HD ~6 nm). The different surface chemistry of the coating ligands (GSH and BSA) on the NCs might also contribute to the difference in their cell uptake. GSH is a zwitterionic ligand with two carboxyl and one amine groups, which might enhance the uptake of the GSH-Au₂₅ NCs by the cells.

In vivo experiments were carried out to further confirm the strong radiation enhancement caused by GSH- or BSA-Au₂₅ NCs. We first labeled GSH- and BSA-Au₂₅ NCs with an organic dye, Cy5, whose excitation and emission wavelengths were 595 and 680 nm, respectively. The Cy5-labeled GSH- and BSA-Au₂₅ NCs also showed red emission peaks at around 680 nm when excited at 595 nm (Figure S2). The *in vivo* pharmacokinetics of GSH- and BSA-Au₂₅ NCs in blood were evaluated using male nude mice bearing the U14 tumor with a tumor weight of ~10 mg-tumor/kg-body. The mice were intraperitoneally injected with Cy5-labeled GSH- or BSA-Au₂₅ NCs (10 mg-Au/kg-body), and the concentrations of GSH- or BSA-Au₂₅ NCs in blood were monitored by their fluorescence over a 24 h period after injection. As shown in **Figure 3a**, the half-life of GSH- and BSA-Au₂₅ NCs in blood was determined to be ~0.25 and 0.75 h, respectively. As compared with the BSA-Au₂₅ NCs, the shorter half-life of GSH-Au₂₅ NCs in blood could be attributed to its much smaller HD. The concentrations of both GSH- and BSA-Au₂₅ NCs in blood were gradually stabilized after ~2.5 h (Figure 3a). The pharmacokinetics of such passive targeting NCs may follow a two-compartment model in which the biocompatible ligands on the NC surface help the NCs in blood penetrate tissues through the transendothelial pores in tumor blood vessels and subsequently deposit in the tumor interstitium.^[18]

The accumulations of GSH- and BSA-Au₂₅ NCs in tumors were further confirmed by the *in vivo* fluorescence imaging (Figure 3b). Strong fluorescence was observed in the tumor site

(indicated by the circle) at 24 h after the injection of Cy5-labeled GSH- or BSA-Au₂₅ NCs. Strong fluorescence was also observed in the liver and bladder. The *in vivo* biodistributions of the injected GSH- and BSA-Au₂₅ NCs were evaluated using the fluorescence intensity of the tissues at 680 nm when excited by a 595-nm laser. Figure 3c shows that the NCs were rarely found in most of the organs except liver and bladder, indicating that the NCs had sufficient transit time in the systemic circulation for the deposition in tumor. The depositions of GSH- and BSA-Au₂₅ NCs in tumors were ~13.1% and 8.6% ID/g (refers to percentage of the injected dose per gram-tissue), respectively. The *in vivo* biodistribution data of the NCs at day 20 after injection (Figure S3) was also investigated by measuring the concentrations of Au in the dissected organs of sacrificed mice bearing the U14 tumors using inductively coupled plasma mass spectrometry (ICP-MS). The Au concentrations in the tumors were ~1456 and 216 ng/g-tumor in mice treated with GSH- and BSA-Au₂₅ NCs, respectively. These values were consistent with the biodistribution data determined from the fluorescence intensity (Figure 3b). It is worth mentioning that the Au NCs used in this study showed improved tumor accumulation relative to that of larger Au NPs.^[19] For example, 6.63% ID/g deposition in tumor was observed for 20 nm PEG-Au NPs, but <1% ID/g in tumor was observed for 80 nm PEG-Au NPs.^[4b] These values were much lower than those of our Au NC systems: 13.1% and 8.6% ID/g in tumors for GSH- and BSA-Au₂₅ NCs, respectively. In addition, the Au concentration in the tumors of mice treated with GSH-Au₂₅ NCs (~1456 ng/g-tumor) was much higher than those reported for Au NP-based systems (e.g., 100–300 ng/g-tumor for 5–50 nm PEG-Au NPs and 100–600 ng/g-tumor for 2–15 nm tiopronin-Au NPs).^[2b, 7, 19b] Taken together, the data suggested that an enhanced uptake by the tumor tissues *via* the improved EPR effect was realized for GSH-Au₂₅ NCs due to their ultrasmall HD and biocompatible surface.

The encouraging results from the *in vitro* radiation therapy and *in vivo* biodistribution studies on GSH- and BSA-Au₂₅ NCs prompted an *in vivo* radiotherapy trial to further evaluate the potential of the new Au NC-based radiosensitizers for clinical use. Twenty-four male and 24 female nude mice bearing the U14 tumor with a tumor weight of ~10 mg-tumor/kg-body were chosen as our animal model. The mice were intraperitoneally injected with GSH- or BSA-Au₂₅ NCs to a concentration of 10 mg-Au/kg-body. After 0.5 h, the mice were irradiated under ¹³⁷Cs gamma radiation of 3600 Ci at a 5 Gy dose. After 20 days, the tumor volumes and weights in the sacrificed mice were measured (**Figure 4a**). As compared with the control group ($p < 0.05$), remarkable decreases of ~55% and ~38% in tumor volume were observed in mice treated with GSH- and BSA-Au₂₅ NCs, respectively. In addition, as compared with the mice treated by radiation only, the tumor volume decreased ~35% and ~10% in mice treated with GSH-Au₂₅ NCs *plus* radiation ($p < 0.05$) and BSA-Au₂₅ NCs *plus* radiation ($p < 0.1$), respectively. Figure 4b shows that the tumor weight decreased in mice treated with GSH- and BSA-Au₂₅ NCs *plus* radiation. Similarly, as compared with the control group ($p < 0.05$), significant tumor weight decreases of 55% and 39% were observed in mice treated with GSH- and BSA-Au₂₅ NCs, respectively. The *in vivo* data further confirmed the strong radiation enhancement from the Au NCs for cancer radiotherapy. In addition, GSH-Au₂₅ NCs showed better accumulation in tumors and therefore stronger enhancement for cancer radiotherapy than the BSA-Au₂₅ NCs.

The promising *in vivo* radiotherapy data of the GSH-Au₂₅ NCs motivated us to study their *in vivo* cytotoxicity, which is pivotal to further developing this new class of radiosensitizer for clinical use. To achieve efficient cancer radiotherapy, the concentration of GSH-Au₂₅ NCs was determined to be 10 mg-Au/kg-body. This concentration was similar to those used in other studies on therapeutic Au NPs [2b, 19a] and was therefore chosen as our model dose. No obvious abnormal organ index and loss of the body weight were observed in mice treated with

GSH-Au₂₅ NCs (Figure S4). **Figure 5a** shows the pathological results for the heart, liver, spleen, lung, and kidney in mice treated with GSH-Au₂₅ NCs, and there were no significant damages in these organs. In contrast, an obvious liver damage was observed in mice treated with BSA-Au₂₅ NCs (Figure 5b and 5c). This damage could be related to the long-term accumulation of BSA-Au₂₅ NCs in liver. Although a certain amount of the Au NCs (coated with GSH or BSA) were also accumulated in the genital system (e.g., testiculus), there were no obvious damages seen in these organs (Figure S5).

To further understand the toxicological response that caused the liver damage in the BSA-Au₂₅ NC system, the hematology and blood biochemistry after 20 days of injection were analyzed (Figure 5b and 5c). The hepatic-related serum chemistry, which was highly related to the liver damage and liver function alternation, was the focus of our analysis. An obvious increase of aspartate aminotransferase (AST) and a distinctive decrease of red blood cell (RBC) were observed in mice treated with BSA-Au₂₅ NCs (without radiation). There were no significant changes in other important indicators for liver injury, including alanine aminotransferase (ALT), albumin (ALB), and globulin (GLOB). Similar effects on the liver damage have recently been reported for the PEG-Au NP system, where the accumulation of PEG-Au NPs in liver could induce abnormal gene expression and lead to liver damage. The long retention time of BSA-Au₂₅ NCs in liver could be attributed to its relatively large HD (~6 nm) because particles in this HD range (>5.5 nm) were difficult to be excreted through renal clearance.^[13] In contrast, GSH-Au₂₅ NCs had much smaller HD (~2.4 nm) and therefore had more efficient renal clearance. This was consistent with the observation that there was no visible toxicity in liver for the GSH-Au₂₅ NC system. The low *in vivo* toxicity of GSH-Au₂₅ NCs further paves its way to potential clinical applications. Studies on the long-term toxicity and more rigorous toxicological evaluation are needed to further advance GSH-Au₂₅ NCs as a new type of *metabolizable* and *efficient* clinical radiosensitizer for cancer radiotherapy.

3. Conclusion

In summary, a new type of radiosensitizer was constructed by integrating ultrasmall Au NCs (<2 nm) with biocompatible coating ligands (GSH and BSA). The new nano-constructs (GSH- and BSA-Au₂₅ NCs) inherit attractive features of both the Au core (strong radiotherapy enhancement from the Au atoms) and the coating shell (good biocompatibility conferred from the coating GSH or BSA). The ultrasmall Au₂₅ NCs with biocompatible coating surface displayed higher tumor accumulation *via* the improved EPR effect and therefore had a stronger enhancement for cancer radiotherapy than that of much larger Au NPs. The enhanced radiotherapy was due to the DNA damage caused by the photoelectric effect and Compton scattering of the Au₂₅ NCs. A remarkable decrease in tumor volume and weight was achieved by using the GSH-Au₂₅ NCs as the radiosensitizer. In addition, the hydrodynamically ultrasmall GSH-Au₂₅ NCs (HD ~2.4 nm) showed very efficient renal clearance and therefore had no obvious toxicity in the body, whereas the hydrodynamically larger BSA-Au₂₅ NCs (HD ~6 nm) could not be efficiently removed by the kidney and therefore caused the liver damage. This work is of interest not only because it presents a new type of promising radiosensitizers that have preferential accumulation in tumors, strong radiotherapy enhancement, and can be metabolized after the treatment, but also because it exemplifies a good approach to improve the biocompatibility of functional nanomaterials by simply using a naturally occurring biomolecule (e.g., GSH) as the coating ligand.

4. Experimental Section

Synthesis and Characterizations of GSH- and BSA-Au₂₅ NCs: The synthesis and purification of GSH- and BSA-Au₂₅ NCs followed published procedures.^[14] In a typical synthesis of GSH-Au₂₅ NCs, GSH in the reduced form (40 μ mol) was mixed with a methanol solution of HAuCl₄ (20 mL, 5 mM) at 4 °C for 30 min. An aqueous solution of NaBH₄ (5 mL, 0.2 M, at 0 °C) was then injected rapidly into the reaction mixture under vigorous stirring. The mixture was allowed to react at 4 °C for 1 h. The precipitate was collected and washed with methanol for three times. The precipitate was then dissolved in water (5 mL), and GSH (30 mg) was added to the solution. The solution was stirred and incubated at 55 °C for 3 h. UV-vis absorption spectroscopy was used to monitor the extent of reaction. In a typical synthesis of BSA-Au₂₅ NCs, an aqueous solution of HAuCl₄ (5 mL, 10 mM, 37 °C) was mixed with a BSA solution (5 mL, 50 mg/mL, 37 °C) under vigorous stirring. After two minutes, NaOH solution (0.5 mL, 1 M) was introduced, and the mixture was incubated at 37 °C for 12 h. Both GSH- and BSA-Au NCs were purified by using dialysis bags with a molecular weight cutoff (MWCO) of 3 kDa. The purified Au NCs were stored in fridge at 4 °C, and were ready for use.

The hydrodynamic diameter (HD) distributions of the as-synthesized Au NCs were determined by dynamic light scattering (DLS) on a NanoZS Zetasizer (Malvern). The DLS data were acquired in the phase analysis light scattering mode at 25 °C, and the sample solutions were prepared by dissolving the Au NCs in 10 mM phosphate-buffered saline (PBS) solution (pH 7.0). The core sizes of the Au NCs were analyzed by transmission electron microscopy (TEM) on a JEM-2100F (JEOL) microscope operating at 200 kV. The UV-vis absorption spectra were recorded on a UV-1800 spectrophotometer (Shimadzu). The photoluminescence (PL) spectra were measured by a F4600 fluorescence spectrophotometer (Hitachi).

Fluorescent Labeling of GSH- and BSA-Au₂₅ NCs: Cy5-SE (Fanbo Biochemicals Co., Ltd. Beijing, China) was used to label Au₂₅ NCs according to a reported procedure.^[18] In a typical modification, the as-synthesized Au₂₅ NCs (1.5 mL, 1 mg-Au/mL) were mixed with Cy5-SE (1.5 mL, 0.1 mg/mL), and the mixture was allowed to react for 24 h in dark. The labeled Au₂₅ NCs were washed several times with copious water by ultrafiltration (2 kDa MWCO membranes) until no obvious blue color was observed in the filtrate.

In vitro Cytotoxicity Test: Hela cells were cultured at 37 °C in humidified atmosphere with 5% CO₂ and low-glucose Dulbecco's modified Eagle's medium (DMEM) which contained fetal calf serum (10%), L-glutamine (2.9 mg/mL), streptomycin (1 mg/mL) and penicillin (1000 units/mL). The cells (in culture medium) were dispensed in 96-well plates (90 µL containing 10⁴ cells per well). Different concentrations of the Au₂₅ NCs (10 µL) were then added to each well. The effect of the concentration of Au₂₅ NCs was assessed using Cell Titre-Glo™ luminescent cell viability assay (Promega, Madison, WI, USA). After 24 or 48 h of treatment, 20 µL of Cell Titre-Glo™ reagent was added and mixed with the mixture in each well on an orbital shaker. The luminescence signal was recorded with a single tube luminometer (TD 20/20, Turner Biosystems Inc., Sunnyvale, CA, USA). The amount of ATP, which was proportional to the number of cells presented in culture, was determined from the assay.

In vitro Radiation Therapy: Hela cells (1 × 10³) were incubated in 25 cm² flasks overnight and then exposed to the Au₂₅ NCs (50 µg-Au/mL) for another 24 h. Cells were then irradiated under gamma-rays from ¹³⁷Cs (photon energy 662 keV) with an activity of 3600 Ci at the doses of 1, 2, 4, 6, and 8 Gy. After irradiation, cells were trypsinized, counted, and seeded in 6 cm dishes with a 5 mL culture medium. Six dishes were prepared for each dose. The cells

were incubated for 10 days and then stained with crystal violet. The as-formed colonies were fixed and the surviving fraction was determined by the ratio of colony numbers in the irradiated cells to that in the untreated cells. Colonies with more than 50 cells were counted. The cell survival curve was fitted using a multi-target single-hit model ($S = 1 - (1 - e^{D/D_0})^N$), where S is the surviving fraction and D is the radiation dose. The value of D_0 was estimated from the fitting, and the sensitization enhancement ratio (SER) was determined by the radiation dose that led to a 50% survival of the cells.

In vitro DNA Break: A modified version of the alkaline COMET-assay protocol was performed to evaluate the DNA break. In a typical assay, frosted microscope slides were covered with 200 μ L of 0.1% agarose in PBS. After the solidification of agarose, 2×10^5 cells suspended in 10 μ L of PBS and 75 μ L of 0.5% low-melting-point agarose were added to each slide. After solidification, the slides were placed in cold fresh lyses buffer [2.5 M NaCl, 100 mM disodium ethylenediaminetetraacetate (EDTA), 10 mM Tris-HCl, and 1% Triton X-100] for 1 h and subsequently in a horizontal gel electrophoresis unit (20 \times 25 cm) filled with chilled electrophoresis buffer (300 mM NaOH and 1 mM Na₂EDTA) for 30 min. Electrophoresis was then conducted at 14 V for 1 h. The slides were drained, neutralized, and dried with ethanol after the electrophoresis. The comets were stained with ethidium bromide. The DNA damage was analyzed using Comet Assay Software Project (CASP) software that measures the tail moment.

In vivo Imaging: All animals were purchased, maintained, and handled using protocols approved by the Institute of Radiation Medicine, Chinese Academy of Medical Sciences (CAMS). The U14 tumor models were generated by subcutaneous injection of 2×10^6 cells suspended in 50 μ L of PBS into the right shoulder of male nude mice. Before the experiments, the mice were anesthetized by chloral hydrate. The Cy5-labeled GSH-Au NCs (150 μ L, 1 mg-

Au/mL) and BSA-Au NCs (150 μ L, 1 mg-Au/mL) were respectively intraperitoneally injected into two groups of male nude mice (three mice per group) at day 7 after the tumor inoculation when the tumor volume reached 100–120 mm³. The Au NCs were then imaged using the *in vivo* fluorescence imaging system (Caliper Inc.). Visible red light with a central wavelength of 595 nm was used as the excitation source. The *in vivo* imaging wavelength range was 610–800 nm with an exposure time of 82 and 76 ms. Autofluorescence was removed using the spectral unmixing software. In the biodistribution and blood concentration measurement, the organ tissues were homogenized in the buffered formalin, and the resultant tissue suspensions were diluted 100 times. The photoluminescence intensity of the samples was measured at the excitation wavelength of 595 nm. The photoluminescence intensities of both standard samples and tissue samples were all adjusted to a linear range. The biodistribution of the Au NCs in the organs of the mice was obtained and plotted with the unit of % ID/g (percentage of the injected dose per gram-tissue).

In vivo Radiation Therapy: All animals were purchased, maintained, and handled using protocols approved by the Institute of Radiation Medicine, CAMS. The U14 tumor models were generated by subcutaneous injection of 2×10^6 cells suspended in 50 μ L of PBS into the right shoulder of BALB/c mice. The mice were intraperitoneally treated with the GSH- and BSA-Au₂₅ NCs when the tumor volume reached 100–120 mm³ (7 days after tumor inoculation). For each treatment, Au₂₅ NCs (1 mg-Au/mL) were intraperitoneally injected at a dosage of 10 mg/kg in the mice. As the control, 200 μ L of saline was intraperitoneally injected into each mouse in the control group. Subsequently, the mice were irradiated by 5 Gy gamma-rays from ¹³⁷Cs (photon energy 662 keV) with an activity of 3600 Ci. 48 mice were assigned to the following six groups (eight mice per group): control, GSH-Au₂₅ NCs, BSA-Au₂₅ NCs, radiation alone, GSH-Au₂₅ NCs + radiation, BSA-Au₂₅ NCs + radiation. Every group includes four male and four female mice in order to monitor the gender difference. The

tumor size was measured every two or three days and calculated using the equation: tumor volume = (tumor length) \times (tumor width)² / 2.

In vivo Toxicity: Mice were weighed and assessed for behavioral changes. At day 20 after the treatment, all mice were sacrificed, and their blood and organs were collected for hematology, biochemistry and toxicological investigation. The blood was drawn for hematology analysis (potassium EDTA collection tube) and serum biochemistry analysis (lithiumheparin collection tube) using a standard saphenous vein blood collection technique. During necropsy, liver, kidney, spleen, heart, lung, brain, genitals, tumor, and thyroid were collected and weighed. The spleen and thymus indexes (S_x) were used to examine the grade of changes caused by malities. The definition of S_x is shown as below:

$$S_x = \frac{\text{Weight of experimental organ (mg)}}{\text{Weight of experimental animal (g)}}$$

Major organs from these mice were then fixed in 4% neutral buffered formalin, processed into paraffin, and stained with hematoxylin and eosin (H&E). Pathology was examined using a digital light microscope. The organs and original solutions of BSA- and GSH-Au₂₅ NCs were digested using a microwave system CEM Mars 5 (CEM, Kamp Lintfort, Germany) to determine their Au content, which was measured on an inductively coupled plasma mass spectrometer (Agilent 7500 CE, Agilent Technologies, Waldbronn, Germany).

Supporting Information

Supporting Information is available online from the Wiley Online Library or from the author.

Acknowledgements

This work is supported by the National Natural Science Foundation of China (Grant No.81000668), Natural Science Foundation of Tianjin (Grant No. 13JCQNJC13500), the Subject Development Foundation of Institute of Radiation Medicine, CAMS (Grant No.SF1207) and Foundation of Union New Star, CAMS. It is also supported with the joint lab of nanotechnology for bioapplication, which was established with Life Technologies Corp. in the National Center for Nanoscience and Technology of China. Part of this work is supported by the Ministry of Education, Singapore, under grant R-279-000-327-112.

References

- [1] a) X. Huang, I. H. El-Sayed, W. Qian, M. A. El-Sayed, *J. Am. Chem. Soc.* **2006**, *128*, 2115; b) D. Kim, S. Park, J. H. Lee, Y. Y. Jeong, S. Jon, *J. Am. Chem. Soc.* **2007**, *129*, 7661; c) K. Sokolov, M. Follen, J. Aaron, I. Pavlova, A. Malpica, R. Lotan, R. Richards-Kortum, *Cancer Res.* **2003**, *63*, 1999; d) R. Elghanian, J. J. Storhoff, R. C. Mucic, R. L. Letsinger, C. A. Mirkin, *Science* **1997**, *277*, 1078; e) J. Chen, F. Saeki, J. Benjamin, H. Cang, M. J. Cobb, Z. Y. Li, L. Au, H. Zhang, M. B. Kimmey, X. Li, Y. Xia, *Nano Lett.* **2005**, *5*, 473; f) N. L. Rosi, D. A. Giljohann, C. S. Thaxton, A. K. R. Lytton-Jean, M. S. Han, C. A. Mirkin, *Science* **2006**, *312*, 1027; g) S. Wang, P. Huang, L. Nie, R. Xing, D. Liu, Z. Wang, J. Lin, S. Chen, G. Niu, G. Lu, X. Chen, *Adv. Mater.* **2013**, doi: 10.1002/adma.201204623; h) N. A. Kotov, F. Stellacci, *Adv. Mater.* **2008**, *20*, 4221; i) T. K. Sau, A. L. Rogach, F. Jäckel, T. A. Klar, J. Feldmann, *Adv. Mater.* **2010**, *22*, 1805; j) H. Cheng, C. J. Kastrup, R. Ramanathan, D. J. Siegwart, M. Ma, S. R. Bogatyrev, Q. Xu, K. A. Whitehead, R. Langer, D. G. Anderson, *ACS Nano* **2010**, *4*, 625; k) M. I. Setyawati, C. Y. Tay, S. L. Chia, S. L. Goh, W. Fang, M. J. Neo, H. C. Chong, S. M. Tan, S. C. J. Loo, K. W. Ng, J. Xie, C. N. Ong, N. S. Tan, D. T. Leong, *Nat. Commun.* **2013**, *4*, 1673.
- [2] a) J. F. Hainfeld, D. N. Slatkin, H. M. Smilowitz, *Phys. Med. Biol.* **2004**, *49*, N309; b) X. D. Zhang, D. Wu, X. Shen, J. Chen, Y. M. Sun, P. X. Liu, X. J. Liang, *Biomaterials* **2012**, *33*, 6408.
- [3] a) R. Jin, *Nanoscale* **2009**, *2*, 343; b) Q. Zhang, J. Xie, Y. Yu, J. Y. Lee, *Nanoscale* **2010**, *2*, 1962; c) Y. Negishi, Y. Takasugi, S. Sato, H. Yao, K. Kimura, T. Tsukuda, *J. Am. Chem. Soc.* **2004**, *126*, 6518; d) Y. Negishi, K. Nobusada, T. Tsukuda, *J. Am. Chem. Soc.* **2005**, *127*, 5261; e) S. Choi, R. M. Dickson, J. Yu, *Chem. Soc. Rev.* **2012**, *41*, 1867.
- [4] a) S. D. Perrault, C. Walkey, T. Jennings, H. C. Fischer, W. C. W. Chan, *Nano Lett.* **2009**, *9*, 1909; b) G. Zhang, Z. Yang, W. Lu, R. Zhang, Q. Huang, M. Tian, L. Li, D. Liang, C.

Li, *Biomaterials* **2009**, *30*, 1928; c) L. Y. T. Chou, W. C. W. Chan, *Adv. Healthcare Mater.* **2012**, *1*, 714.

[5] Y. J. Li, A. L. Perkins, Y. Su, Y. Ma, L. Colson, D. A. Horne, Y. Chen, *Proc. Natl. Acad. Sci. U. S. A.* **2012**, *109*, 4092.

[6] a) Y. Wang, Y. Liu, H. Luehmann, X. Xia, P. Brown, C. Jarreau, M. Welch, Y. Xia, *ACS Nano* **2012**, *6*, 5880; b) L. Balogh, S. S. Nigavekar, B. M. Nair, W. Lesniak, C. Zhang, L. Y. Sung, M. S. T. Kariapper, A. El-Jawahri, M. Llanes, B. Bolton, F. Mamou, W. Tan, A. Hutson, L. Minc, M. K. Khan, *Nanomed:NBM.* **2007**, *3*, 281.

[7] K. Huang, H. Ma, J. Liu, S. Huo, A. Kumar, T. Wei, X. Zhang, S. Jin, Y. Gan, P. C. Wang, S. He, X. Zhang, and X. J. Liang, *ACS Nano* **2012**, *6*, 4483.

[8] a) A. Verma, F. Stellacci, *Small* **2009**, *6*, 12; b) A. Verma, O. Uzun, Y. Hu, Y. Hu, H. S. Han, N. Watson, S. Chen, D. J. Irvine, F. Stellacci, *Nat. Mater.* **2008**, *7*, 588.

[9] a) C. Zhou, M. Long, Y. Qin, X. Sun, J. Zheng, *Angew. Chem. Int. Ed.* **2011**, *123*, 3226; b) C. Zhou, G. Hao, P. Thomas, J. Liu, M. Yu, S. Sun, O. K. Öz, X. Sun, J. Zheng, *Angew. Chem. Int. Ed.* **2012**, *124*, 10265.

[10] X. D. Zhang, D. Wu, X. Shen, P. X. Liu, F. Y. Fan, S. J. Fan, *Biomaterials* **2012**, *33*, 6408.

[11] a) J. Yu, S. Choi, R. M. Dickson, *Angew. Chem. Int. Ed.* **2009**, *121*, 324; b) J. Yu, S. A. Patel, R. M. Dickson, *Angew. Chem. Int. Ed.* **2007**, *119*, 2074; c) Y. Zhang, F. Zheng, T. Yang, W. Zhou, Y. Liu, N. Man, L. Zhang, N. Jin, Q. Dou, Y. Zhang, *Nat. Mater.* **2012**, *11*, 817.

[12] a) W. H. De Jong, W. I. Hagens, P. Krystek, M. C. Burger, A. J. A. M. Sips, R. E. Geertsma, *Biomaterials* **2008**, *29*, 1912; b) J. Lipka, M. Semmler-Behnke, R. A. Sperling, A. Wenk, S. Takenaka, C. Schleh, T. Kissel, W. J. Parak, W. G. Kreyling, *Biomaterials* **2010**, *31*, 6574.

- [13] H. S. Choi, W. Liu, P. Misra, E. Tanaka, J. P. Zimmer, B. I. Ipe, M. G. Bawendi, J. V. Frangioni, *Nat. Biotech.* **2007**, *25*, 1165.
- [14] a) J. Xie, Y. Zheng, J. Y. Ying, *J. Am. Chem. Soc.* **2009**, *131*, 888; b) Y. Shichibu, Y. Negishi, H. Tsunoyama, M. Kanehara, T. Teranishi, T. Tsukuda, *Small* **2007**, *3*, 835.
- [15] M. Zhu, C. M. Aikens, F. J. Hollander, G. C. Schatz, R. Jin, *J. Am. Chem. Soc.* **2008**, *130*, 5883.
- [16] Y. Shichibu, Y. Negishi, T. Tsukuda, T. Teranishi, *J. Am. Chem. Soc.* **2005**, *127*, 13464.
- [17] Z. Wu, R. Jin, *Nano Lett.* **2010**, *10*, 2568.
- [18] L. Cheng, K. Yang, Q. Chen, Z. Liu, *ACS Nano* **2012**, *6*, 5605.
- [19] a) G. von Maltzahn, J. H. Park, A. Agrawal, N. K. Bandaru, S. K. Das, M. J. Sailor, S. N. Bhatia, *Cancer Res.* **2009**, *69*, 3892; b) X. Huang, X. Peng, Y. Wang, D. M. Shin, M. A. El-Sayed, S. Nie, *ACS Nano* **2010**, *4*, 5887.

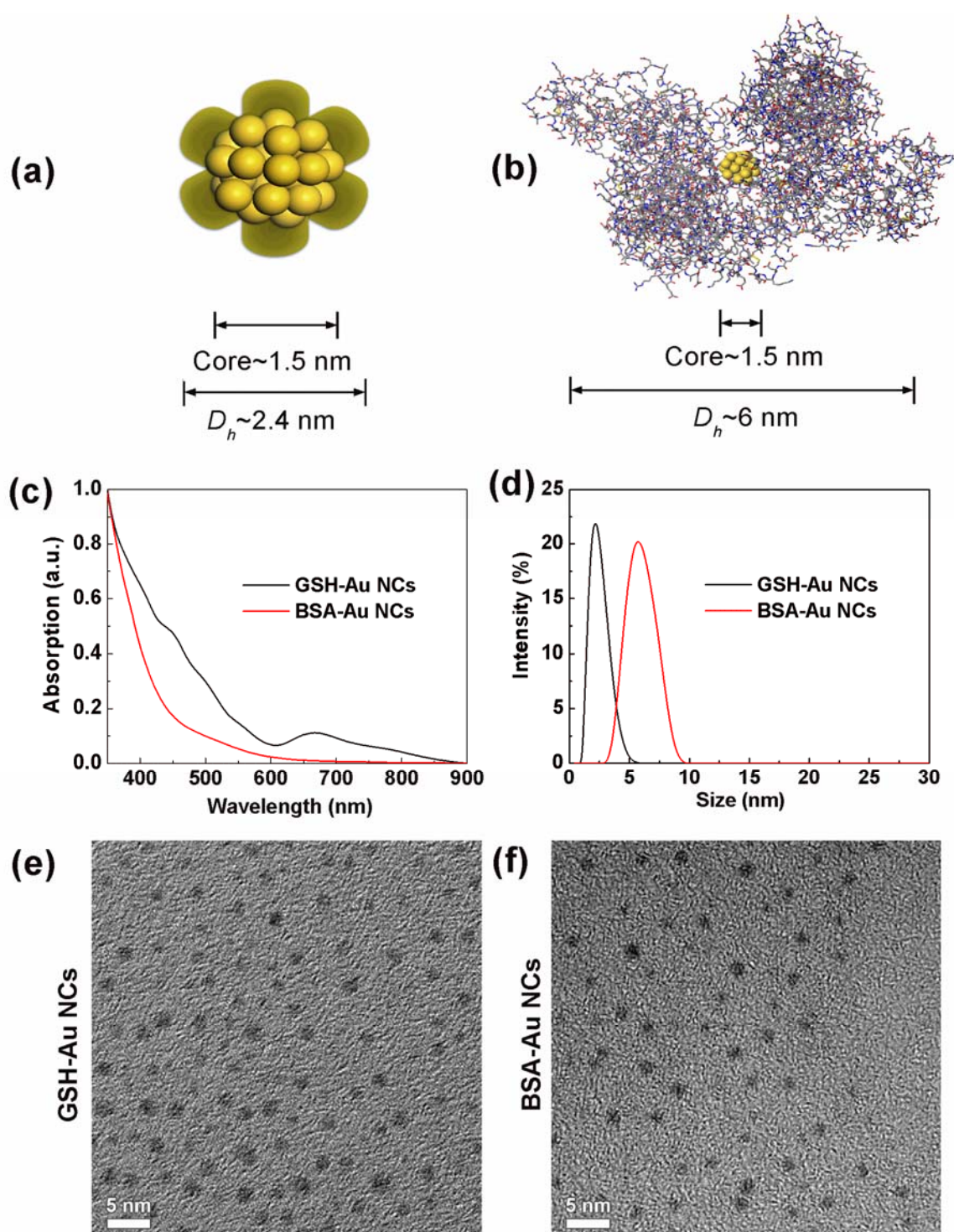


Figure 1. Schematic illustration of the core-shell structure of (a) GSH-Au₂₅ NCs and (b) BSA-Au₂₅ NCs. (c) UV-vis and (d) DLS spectra of the as-prepared GSH-Au₂₅ NCs (black line) and BSA-Au₂₅ NCs (red line). Representative TEM images of the as-prepared (e) GSH-Au₂₅ NCs and (f) BSA-Au₂₅ NCs.

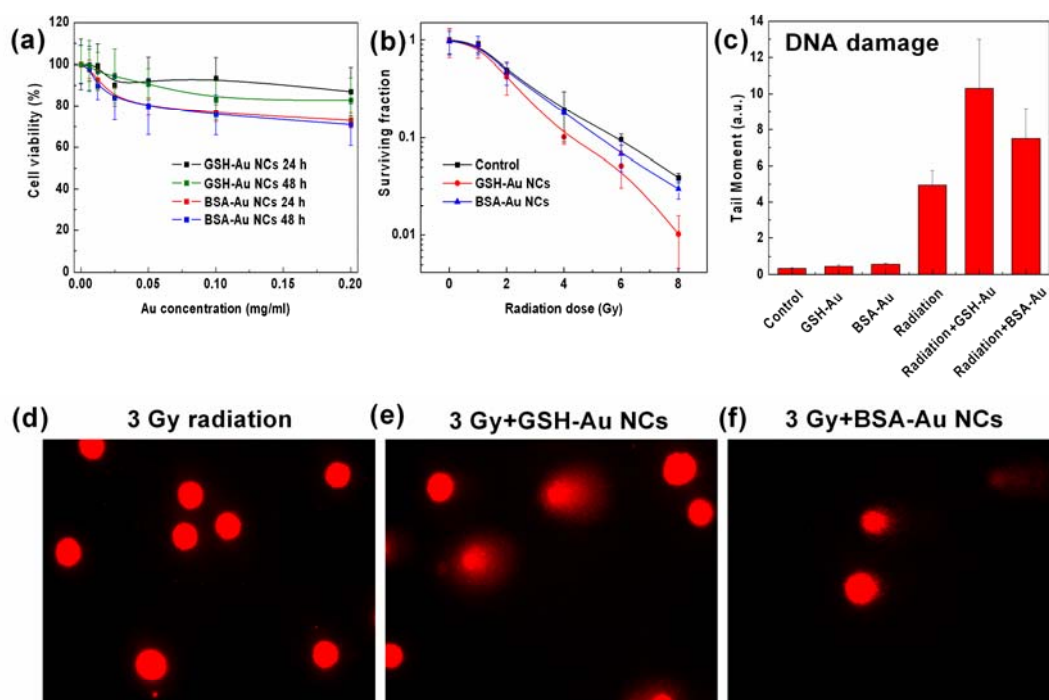


Figure 2. (a) Viability of HeLa cells after incubation with GSH- and BSA-Au₂₅ NCs for 24 and 48 h. (b) Viability of HeLa cells treated with only radiation (control, black line), GSH-Au₂₅ NCs (50 µg-Au/mL) + radiation (red line), and BSA-Au₂₅ NCs (50 µg-Au/mL) + radiation (blue line). (c) Tail moment of HeLa cells treated with GSH-Au₂₅ NCs, BSA-Au₂₅ NCs, radiation (3 Gy), GSH-Au₂₅ NCs + radiation (3 Gy), and BSA-Au₂₅ NCs + radiation (3 Gy). Representative cell images of fluorescent DNA stain of (d) radiation group, (e) GSH-Au₂₅ NCs + radiation (3 Gy), and (f) BSA-Au₂₅ NCs + radiation (3 Gy).

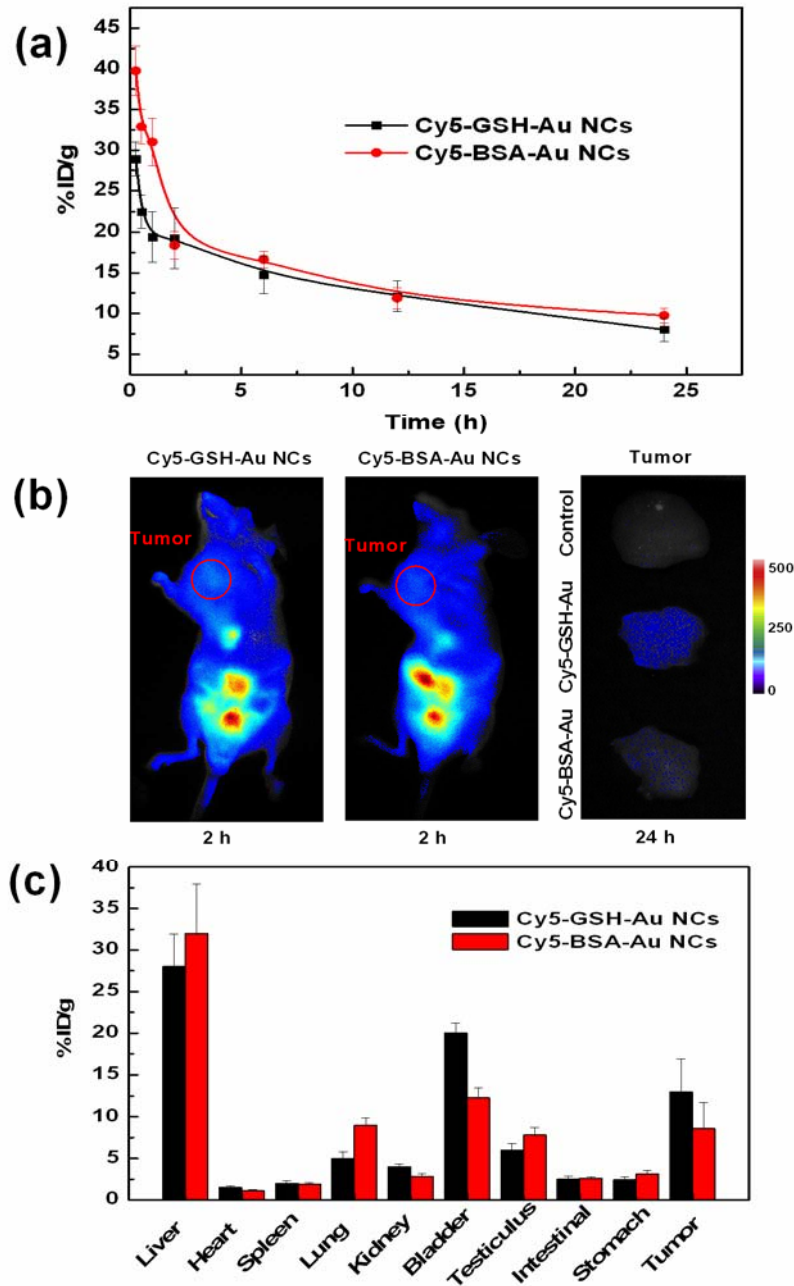


Figure 3. (a) *In vivo* pharmacokinetic studies of GSH-Au₂₅ NCs (black line) and BSA-Au₂₅ NCs (red line). (b) Fluorescence images of mice treated with GSH-Au₂₅ NCs (left panel) and BSA-Au₂₅ NCs (middle panel) at 2 h after injection; the right panel is the tumor images (false color) at 24 h after injection of the control group (top), GSH-Au₂₅ NCs group (middle), and BSA-Au₂₅ NCs group (down). (c) Biodistribution of GSH-Au₂₅ NCs (black column) and BSA-Au₂₅ NCs (red column) at 24 h after injection.

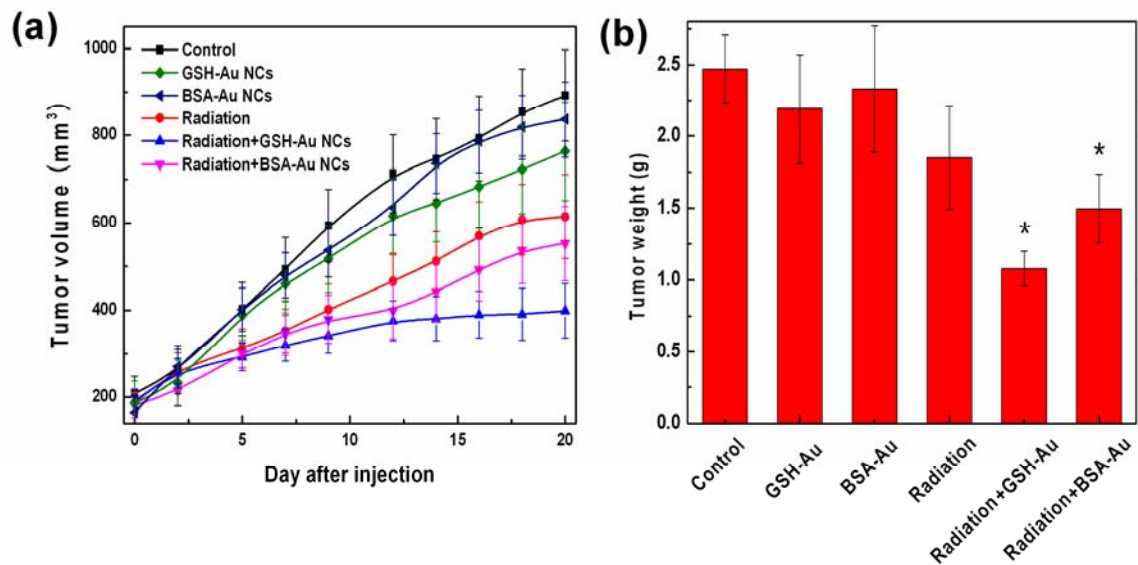


Figure 4. Time-course studies of tumor (a) volumes and (b) weights of mice treated with GSH- and BSA-Au₂₅ NCs at the concentration of 10 mg-Au/kg-body. Data was analyzed by Student's t-test and * in (b) indicates $p < 0.05$.

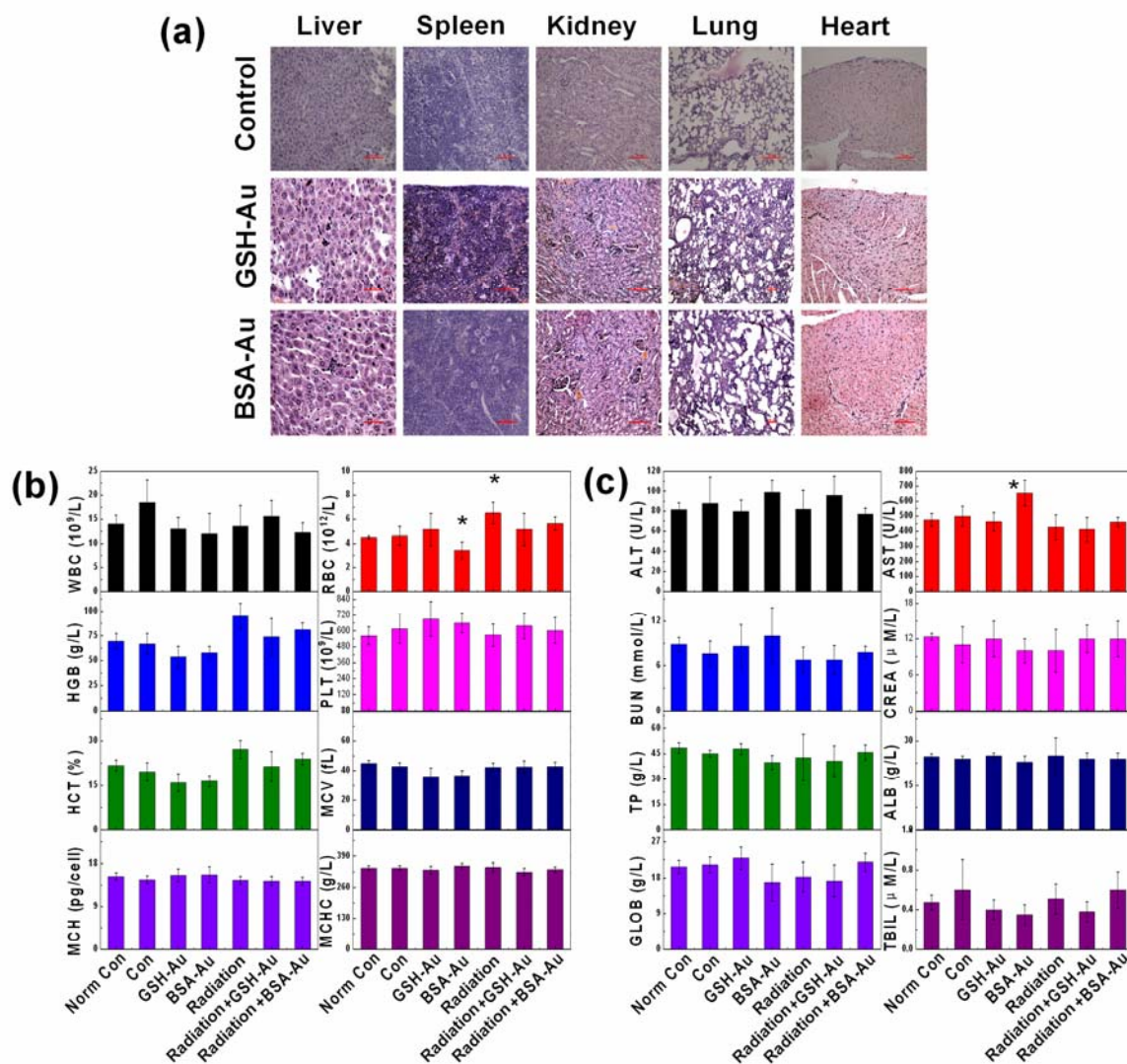


Figure 5. (a) Pathological data from the liver, spleen, kidney, lung, and heart of mice treated with GSH- and BSA-Au₂₅ NCs at the concentration of 10 mg-Au/kg-body. (b) Hematology data of mice treated with GSH- and BSA-Au₂₅ NCs at day 20 after injection. The results show mean and standard deviation of white blood cells (WBC), RBC, hematocrit (HCT), mean corpuscular volume (MCV), hemoglobin (HGB), platelets (PLT), mean corpuscular hemoglobin (MCH), and mean corpuscular hemoglobin concentration (MCHC). (c) Blood biochemistry analysis of mice treated with GSH- and BSA-Au₂₅ NCs at day 20 after injection. The results show mean and standard deviation of ALT, AST, total protein (TP), ALB, blood urea nitrogen (BUN), creatinine (CREA), GOLB, and total bilirubin (TB). Data was analyzed by Student's t-test and * in (b) and (c) indicates $p < 0.05$.

Supporting Information

Enhanced Tumor Accumulation of Sub-2 nm Gold Nanoclusters for Cancer Radiation Therapy

X. Zhang, J. Chen, Z. Luo, D. Wu, X. Shen, S. Song, Y. Sun, P. Liu, J. Zhao, S. Huo, S. Fan, F. Fan, X. Liang, and J. Xie **

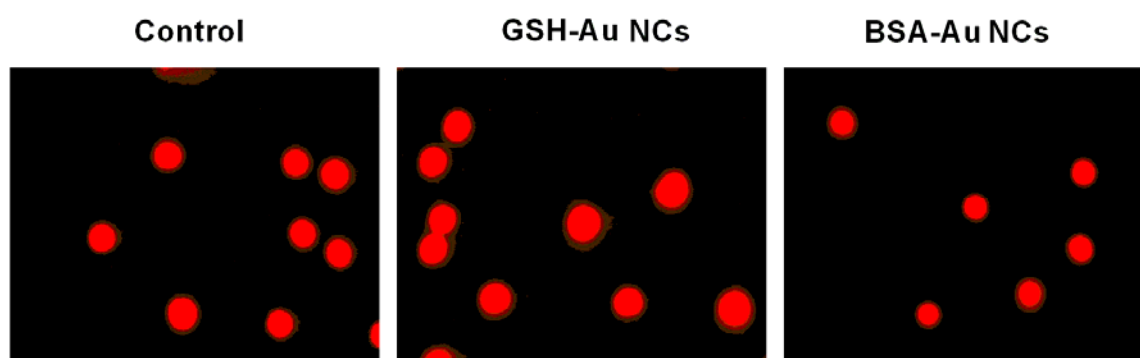


Figure S1. Representative images of fluorescent DNA stain of (a) untreated cells (control group) and cells treated by (b) GSH-Au₂₅ NCs and (c) BSA-Au₂₅ NCs (50 μ g-Au/mL).

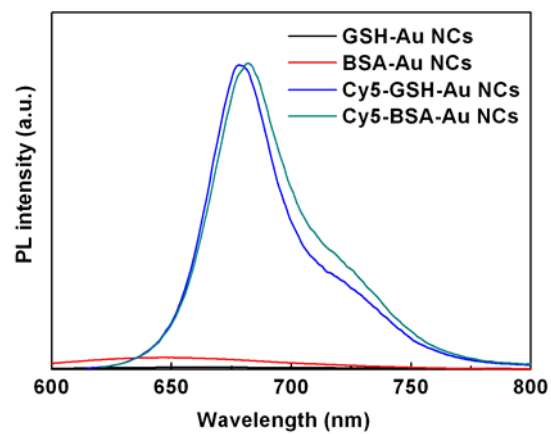


Figure S2. Photoemission spectra of Au₂₅ NCs with and without Cy5 labeling.

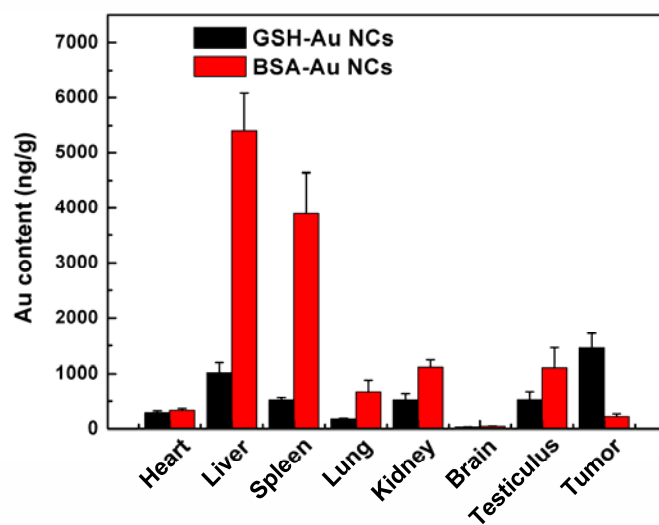


Figure S3. The biodistribution (in terms of Au content, determined by ICP-MS) of GSH- and BSA-Au₂₅ NCs at day 20 after the injection of the NCs.

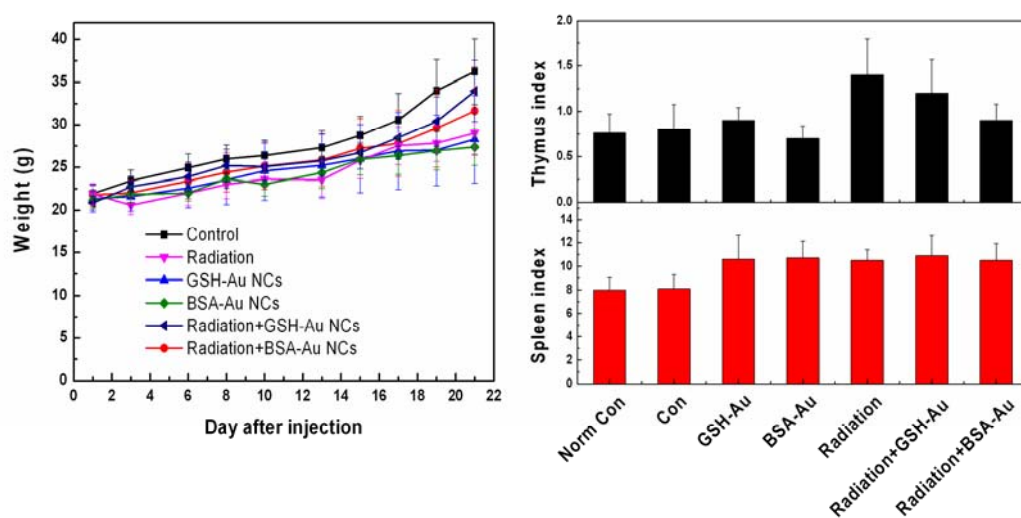


Figure S4. Body and organ index of the GSH- and BSA-Au₂₅ NCs.

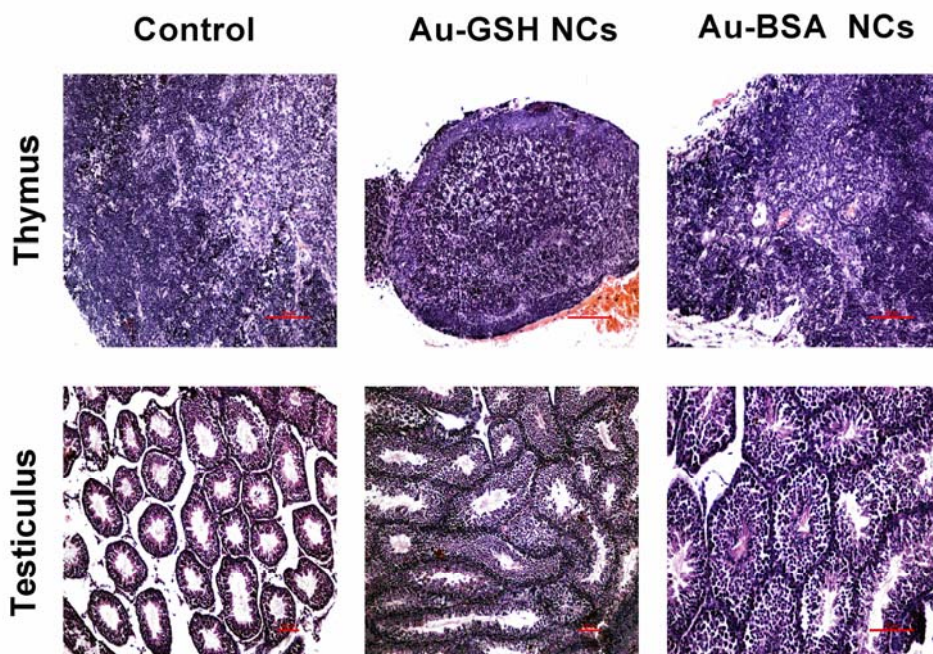


Figure S5. Pathological image of the thymus and testiculus from the untreated mice (control group) and the mice treated with GSH- and BSA-Au₂₅ NCs.